

Simultaneous Scanning Ion Conductance Microscopy and Atomic Force Microscopy with Microchanneled Cantilevers

Dario Ossola, Livie Dorwling-Carter, Harald Dermutz, Pascal Behr, János Vörös, and Tomaso Zambelli*
Laboratory of Biosensors and Bioelectronics, Institute for Biomedical Engineering, ETH Zurich, CH-8092 Zurich, Switzerland
 (Received 8 July 2015; published 3 December 2015)

We combined scanning ion conductance microscopy (SICM) and atomic force microscopy (AFM) into a single tool using AFM cantilevers with an embedded microchannel flowing into the nanosized aperture at the apex of the hollow pyramid. An electrode was positioned in the AFM fluidic circuit connected to a second electrode in the bath. We could thus simultaneously measure the ionic current and the cantilever bending (in optical beam deflection mode). First, we quantitatively compared the SICM and AFM contact points on the approach curves. Second, we estimated where the probe in SICM mode touches the sample during scanning on a calibration grid and applied the finding to image a network of neurites on a Petri dish. Finally, we assessed the feasibility of a double controller using both the ionic current and the deflection as input signals of the piezofeedback. The experimental data were rationalized in the framework of finite elements simulations.

DOI: 10.1103/PhysRevLett.115.238103

PACS numbers: 68.37.Ps, 87.85.Pq

Atomic force microscope (AFM, [1]) is an established imaging instrument for cell biology [2]. However, imaging of soft samples like cells is a challenging task for the AFM. The feedback input is related to the interaction between the hard pyramidal tip and the underlying substrate. In the case of cells, the image contrast is thus determined by the rigid submembrane structures [3]. Scanning ion conductance microscope (SICM, [4]) uses pulled glass pipettes for the surface topography exploiting as the feedback input the ionic current between an electrode in the pipette and one in the bath solution, which depends on the separation from the underlying substrate. Soft structures are imaged in an electrolyte without mechanical contact [4,5]. For living cells under near-physiological conditions, the lateral resolution of SICM, determined by 3 times the inner opening radius of the pipette probe [6], is slightly better than the AFM [7]. The SICM was further developed to improve its performances like the ac mode [8] and the backstep or hopping modes [7,9–11]. Yet, the latter mode implies mapping instead of scanning.

Because of the attractiveness of combining the advantages of the two complementary instruments, SICM and AFM, several strategies were contrived to equip glass pipettes with a force feedback: they are mounted on tuning forks [12–14], but the derivation of the value of z component of the applied force is cumbersome [15]; bent glass micropipettes, e.g., the fountain pen micropipette [16,17], are equipped with a mirror such that a reflected laser could detect their in-plane vibration [18]. Nevertheless, no SICM experiments with these methods are documented in the literature. An original innovation of hybrid SICM was presented by Drake *et al.* [19] where the glass micropipette is suspended with an ingenious leverage system, whose displacement is also monitored with laser

reflection and operated in static and dynamic mode but without quantifying the pipette-substrate interaction.

Taking advantage of the microchanneled AFM cantilevers of the FluidFM [20] having an hollow pyramidal tip and an aperture at its apex (Fig. 1), instead of glass pipettes, we achieved simultaneous AFM and SICM recording.

Similar to conventional SICM, the resulting ionic current was measured upon application of a potential across two Ag/AgCl electrodes [Fig. 1(a)]: the one inserted in the fluidic circuit of the FluidFM, the other in the bath

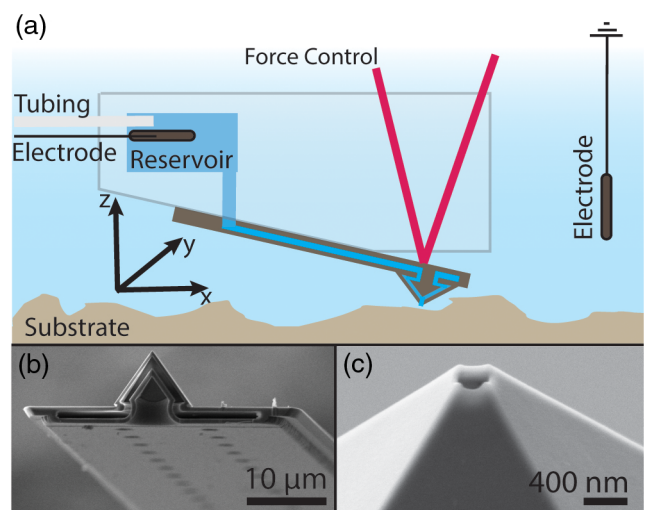


FIG. 1 (color online). (a) Schematics of the FluidFM with Ag/AgCl electrodes for ionic current recording through the embedded microchannel. (b) SEM micrograph of a FIB cross-sectioned cantilever showing the embedded 1- μm high microchannel. (c) SEM micrograph of the 300-nm aperture of an Apex300 probe.

solution (150 mM KCl, unless otherwise stated). The ionic current through the microchanneled cantilever was monitored with a patch clamp amplifier (HEKA EPC7). A FluidFM Apex300 pyramidal probe [Figs. 1(b) and 1(c)] (microchannel section $30 \times 1 \mu\text{m}^2$, aperture diameter 300 nm, stiffness $k \sim 1.9 \text{ N/m}$ determined with the Sader method [21]) immersed in 150 mM KCl showed a typical electrical resistance in the order of $30 \text{ M}\Omega$ and a capacitance of about 15 pF, where the resistance is mainly ($\sim 90\%$) due to the $\sim 2\text{-mm}$ long microchannel rather than to the hollow pyramid and the submicron aperture [22]. A conventional glass micropipette of the same aperture diameter typically shows a lower resistance of 1–20 $\text{M}\Omega$ with a capacitance of 5 to 15 pF.

In this configuration, we can now record simultaneously both the deflection of the cantilever (AFM optical beam detection [23]) as well as the ionic current (SICM). Lateral forces could also be measured through the cantilever torque, but only normal forces are considered in the present Letter.

First, we carried out a force spectroscopy experiment to compare the contact point measured from force and ionic current approach curves. The curves were obtained with an Apex300 probe on a glass surface. The ionic current has been normalized to the maximum ionic current (I_{sat}) measured at far distance. Distant from the substrate, both curves are constant. While starting interacting with the substrate, the slopes change (increase of the deflection because of the repulsion, decrease of the ionic current because of the aperture occlusion). The ionic current amplitude drops about 150 nm before the deflection rises (Fig. 2). To our knowledge, this is the first time that SICM and AFM approach curves were simultaneously measured with the same hollow probe confirming that SICM is indeed noncontact. On polydimethylsiloxane (PDMS, Fig. S1 [24]), the ionic current vs vertical distance is

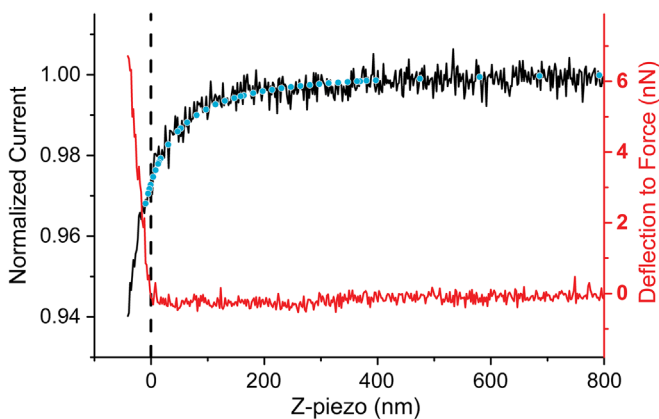


FIG. 2 (color online). Simultaneous force and ionic current spectroscopy with an Apex300 FluidFM probe. Cantilever and bath were filled with 150 mM KCl solution. Overlaid on the ionic current curve is the FEM simulated approach curve (blue dots). At the contact point, the slope of the ionic current was $0.04\%/nm$.

similar to that on glass because both substrates have the same surface charge [29], whereas the deflection curve is indeed different because PDMS is much softer than glass. Hence, force spectroscopy delivers mechanical and electrical information with one single inquiry.

While the aperture of the Apex300 probes was fabricated with a standard lithography process [30], a focused ion beam (FIB) enables us to arbitrarily shape closed FluidFM pyramidal tips [31] reaching aperture diameters down to 20 nm (Fig. S2). Pulled glass pipettes with aperture diameter down to 10 nm exhibit prohibitive electrical impedances in the $\text{G}\Omega$ range [32] compared to $\sim 50 \text{ M}\Omega$ for a custom FluidFM probe with same aperture size. This smaller aperture size resulted in steeper ion-conductance approach curve (Fig. S2, $S_{\text{APEX}} = 0.6 \text{ pA/nm}$ vs $S_{\text{Custom}} = 2.0 \text{ pA/nm}$ at the contact point).

The slope of the ionic current drop was analyzed by finite element (FEM) simulations inspired by the work of Rheinlaender *et al.* [6], also based on FEM to estimate the total current and current density distribution through a glass micropipette when approaching a sample (blue dots overlaid on the experimental SICM curve of Fig. 2). We emphasize that these simulated curves do not include any fitting parameter. Thus, FEM simulations agree with the FluidFM experimental data. This is an inciting finding because the FEM simulations help to assess the impact of the FluidFM aperture geometry on sensitivity and resolution and thus to foresee the experimental results. Despite a geometry different from the conic shape of conventional glass pipettes, microchanneled cantilevers behave like them according to Rheinlaender's approach for image formation and resolution, allowing us to exploit the knowledge already acquired on SICM pipettes. Indeed, FEM simulations for FluidFM probes reveal a comparable lateral resolution of 3 times the aperture inner radius (Fig. S3) [6].

The FluidFM can be operated in SICM mode by switching from the AFM photodiode to the amplified ionic current as the input of the feedback controller. Hence, the next step of our work was to characterize the SICM imaging of a surface with simultaneous AFM recording. As an initial substrate, we chose a calibration grid because of its well-defined geometry featuring 500-nm deep and $2\text{-}\mu\text{m}$ wide trenches. The calibration grid was made of PDMS molded from a silicon test structure (Mikromasch, TGXYZ03 test structure). DC SICM mode monitoring the amplitude of a dc ionic current through the SICM probe, is the simplest and fastest imaging mode. Figure 3 shows the topography of the calibration grid in 150 mM KCl with 20 mV bias applied and scanned at $5 \mu\text{m/s}$ from right to left over a $15 \times 15 \mu\text{m}^2$ area.

The topography mirrors the specimen geometry and dimension [Fig. 3(a)]: slope of the profile across the hill-valley transition measured at the median of the averaged scan profiles is $\Delta z/\Delta x_{\text{UPWARDS}} = 0.62$ and $\Delta z/\Delta x_{\text{DOWNWARDS}}$ measures 0.51, which corresponds to the shape of the tip.

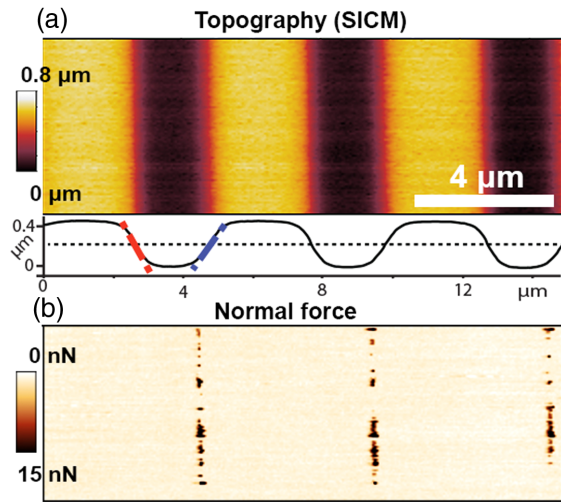


FIG. 3 (color online). $15 \times 5 \mu\text{m}^2$ DC-SICM scan, voltage bias: 20 mV, scan speed: $5 \mu\text{m/s}$, bath solution: 150 mM KCl. Fast scan direction: right to left. (a) Topography. Inset: averaged profile of the topography. (b) Probe-surface interaction force while scanning.

Measured height was 455 nm with an error of 9% compared to the nominal value of 500 nm, whereas the fabricant acknowledges 3% error. Two explanations are plausible: (i) due to limited SICM lateral resolution, topography steps appear smeared out [6,33,34], (ii) given the rather big FluidFM pyramidal tip half angle, the ionic current may decrease due to the confinement in the trench leading to the tip retraction (smaller height). Together with the topography (*i.e.*, piezo displacement), the SICM error as well as the normal and lateral deflection were recorded. The error signal (*i.e.*, the current) confirms the good controller performance as the error deviation is buried in the noise (Fig. S4). During the acquisition time of the image, the deflection signal can be monitored in real time on a separate channel. Normal deflection data reveal measurable contact of the probe with the substrate while moving from the top of the feature into the valley [Fig. 3(b)]. This information helps to guess the tip-substrate separation favoring prolonged operation in the conditions of maximum resolution despite drifts in the dc current. During a conventional SICM experiment, the current setpoint is often chosen blindly so that probe collisions may occur without perception in the search for high resolution. The force generated by a collision is proportional to the stiffness of the probe. When using glass pipettes, which are stiff, these forces are consequently high with possible damaging of the sample and/or the probe. This is the reason why most users prefer the hopping mode SICM where each pixel is acquired by a vertical approach. Whilst solving the above described issue, the acquisition time drastically increases stimulating technical expedients like a second added piezo [35].

In contrast, a FluidFM probe is 2 orders of magnitude softer, its flexibility allows for the FluidFM operation in

dc-SICM mode with smaller damage risks, therefore reducing the image acquisition time. The FluidFM in dc-SICM mode can indeed image soft samples that cannot be otherwise imaged by AFM, at a faster speed than most SICM setups running in hopping mode. To demonstrate such a statement, we imaged a challenging biological specimen. We selected a network of neurites of rat hippocampal neurons [Fig. 4(a)], a challenging biological specimen for the following two reasons: (i) such filamentous cellular structures are nearly impossible to be scanned with AFM also in the gentlest intermittent contact mode because the loosely attached neurites are unavoidably displaced by the pyramid [7]; (ii) our available Z piezo has a $10\text{-}\mu\text{m}$ limit, which is too short to follow the contour of the neuron body. The $50 \times 50 \mu\text{m}^2$ image of Fig. 4 was taken with a scan rate of $13 \mu\text{m/s}$ resulting in 16 min acquisition time of both trace and retrace images. To correct for drifts of the ionic current during scanning, the setpoint was manually adapted to keep a constant interaction force with the sample. Neurite features in the intricate 3D network are clearly distinguishable while no apparent damage and displacement of neurites is noticeable during scanning [refer to trace and retrace profiles, Fig. 4(b)]. The force signal does not exceed 30 nN: the presence of mechanical interaction is due to the choice of the smallest current setpoint striving for maximal spatial resolution (Fig. S5). Scanning in dc mode means higher scanning speeds: the acquisition time of a $50 \times 50 \mu\text{m}^2$ image with 256×256 lines was reduced to 4 min (Fig. S6). As shown in the Supplemental Material [24], the resolution starts deteriorating at scan rates of $50 \mu\text{m/s}$, where scan-involved forces become considerably high.

Both dc and ac modes were assessed in this study (Fig. S7). Ac mode was carried out at 370 Hz with 20 to 60 nm oscillation at the free end of the cantilever. A lock-in amplifier was used to demodulate the amplitude of the

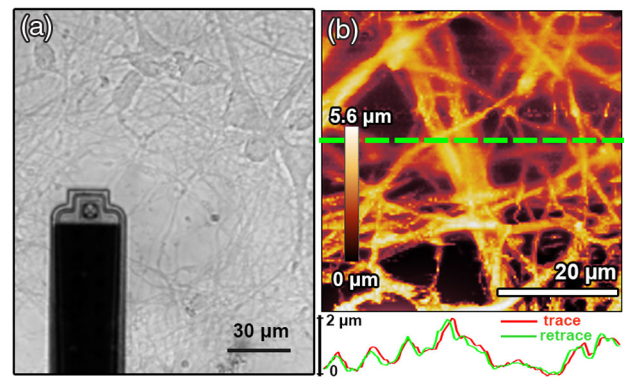


FIG. 4 (color online). Living hippocampal neurons *in vitro*. (a) Optical micrograph of the FluidFM cantilever in proximity of the neurons. (b) 3D representation of the DC-SICM topography showing an intricate 3D-network. Trace (right to left) and retrace profiles are shown in the lower inset below showing good correlation meaning negligible lateral displacement of the neurites.

ac signal. The low excitation frequency is dictated from the relatively low electrical bandwidth of the system ($f_{\text{cutoff}} = \sim 800$ Hz). Nonetheless, in our case, the ac mode performed worse than the dc mode in terms of sensitivity ($S_{\text{DC}} = 0.65$ pA/nm vs $S_{\text{AC}} = 0.04$ pA/nm, Fig. S4). It may be related to the lower probe stiffness in comparison with glass micropipettes: cantilever oscillation amplitude, which is dependent on probe-substrate distance (AFM dynamic mode), is thus affected reducing the sensitivity of the ac signal.

Custom FIB probes with apertures down to 10 nm showed increased sensitivity close to the contact point ($S_{\text{FIB}} = 0.24\%/nm$ vs $S_{\text{Apex300}} = 0.02\%/nm$, Fig. S2). However, the 450-nm thick walls of the pyramid surrounding the aperture compromise the lateral resolution.

In Figs. 3 and 4, the cantilever deflection represented an additional information during scanning in pure SICM mode. The final step of our work was to develop a combined imaging mode using also the measured force as a feedback signal. We aimed to profit from the non-contact SICM imaging on a “smooth” surface, whilst switching to the force feedback on steep obstacles as soon as the measured deflection exceeds a defined at value.

As a first attempt, we evaluated the “safe-tip” option. This protocol automatically retracts the probe by a certain distance with a given speed when a predetermined force threshold is trespassed, preventing a too high tip-substrate interaction. Efficacy of the safe-tip method is shown by imaging a PDMS calibration grid featuring 1 μm deep and 2 μm wide trenches. Figure 5 shows the resulting image where the safe-tip option has been enabled and disabled. Comparing the topography traces in the two cases reveals that the probe is retracted earlier in the proximity of the upwards step as confirmed by the deflection signal (reduction of about 30 nN). Indeed, interaction forces are considerably reduced when the option safe-tip is enabled. Topography profiles show that the estimation of the groove width is overestimated while imaging in SICM mode, a known effect [6], whilst with the safe-tip option enabled the dimension estimation results to be more precise (4.22 μm vs 3.98 μm calculated from the averaged profile. Nominal width: 4 μm). The maximum involved forces are reduced from 37.6 to 8.7 nN with the safe-tip protection. The valley to top slope improved from $\Delta z/\Delta x = 0.73$ to $\Delta z/\Delta x = 1.20$ getting closer to real dimensions. Once the safe-tip option disabled, the same topography profiles were recovered as at the beginning of the experiment (in terms of profile height and lateral resolution, not shown): the reduction in the interaction force is indeed a consequence of the safe-tip strategy and not due to a drift in the ionic current.

As a next step, we examined the simultaneous running of both the AFM and SICM controllers: we added the two output signals of the AFM and SICM amplifiers as the input signal for the feedback loop modulated with different

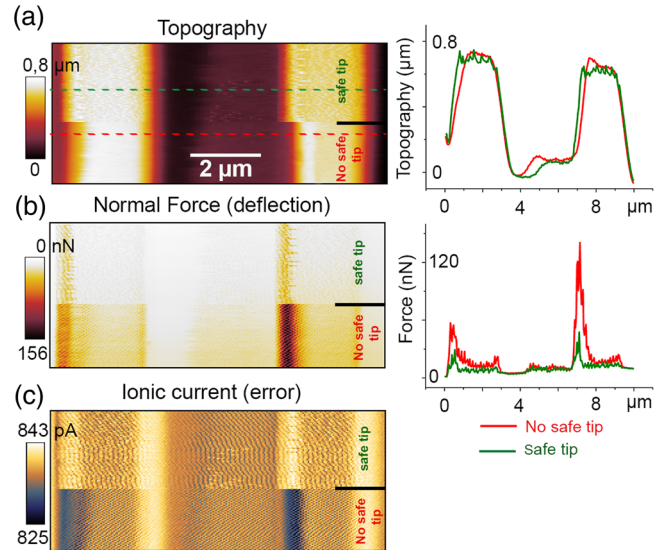


FIG. 5 (color online). Performance of the “safe tip” option acquired in 150 mM KCl at 10 $\mu\text{m}/s$. Voltage bias applied: 29 mV (a) Topography. Height profiles following the dashed lines (red: no safe tip; green: safe tip enabled) are shown on the right panel. (b) Normal force (deflection). Normal force substrate and probe interaction reveals a reduction from ~ 130 nN to about 30 nN demonstrating efficacy of the proposed methodology (red and green profiles on the right panel). Those profiles were extracted from the same lines as in (a). (c) Ionic current, *i.e.*, error of the SICM controller. “Safe tip” intervention is noticeable when the probe is scanning uphill. Indeed, if “safe tip” is disabled, the SICM controller fails to maintain the desired distance from the substrate, consequently, the probe touches the substrate [see the peak in the deflection signal and the drop in the ionic current (~ 820 pA)]. If “safe tip” is enabled, the probe withdrawal is forced at this critical point. Consequently, the probe does not collide as in the deflection signal, but is retracted so that more ionic current flows (~ 840 pA).

weights, $\text{Hybrid}_{\text{in}} = a * \text{AFM}_{\text{out}} + b * \text{SICM}_{\text{out}}$. With Simulink, we analyzed this configuration and validated it experimentally (Fig. S8). The SICM controller was configured to be the leading controller, whereas the AFM controller was configured to be a P controller with the smallest setpoint and high gain (the P controller tolerates a steady-state error, but promptly reacts to a transient perturbation). The latter takes control when a collision is detected. Even though this approach gave promising results by reducing the interaction force peak by ~ 9 nN on a well-known substrate geometry, we faced instability problems. Indeed, the unknown role of bandwidth and phase on the controller output led to unpredictable results and difficult tuning. Further comprehensive plant modeling and controller design will be required for proper operation.

In conclusion, we scanned a surface with microchanneled AFM cantilevers acquiring simultaneously the AFM and SICM signals. The information about the force allows us to determine the tip-substrate separation avoiding unwanted collisions. This method will contribute to studies

in the emerging single-cell research field as it will enable gentle imaging of the cells followed by local perturbation and manipulation with the same probe. Current positioning resolution is on the order of 1 μm , but by combining FIB and microfabrication of thinner pyramidal walls, a resolution of 50 nm can be targeted.

This work was supported by an Interdisciplinary Grant of the Swiss National Science Foundation SNSF (Contract No. “CR23I2_135535”) and the EuroBIOSAS ICS Initiative, FP7 Union’s Seventh Framework Program, Future and Emerging Technologies, Grant Agreement No. 296590). We are indebted to Alessandro Pioda (SPECS Zurich GmbH, CH) for supplying the Nanonis controller and his technical help, to the personnel of ETH ScopeM facility, Edin Sarajlic (SmartTip BV, NED), Patrick Frederix (Nanosurf AG, CH), Michael Gabi, and Pablo Dörig (Cytosurge AG, CH) for their constant support as well as to Stephen Wheeler and Martin Lanz (LBB) for their technical skills. Finally, we are thankful to Professor Jean-Marc Fritschy and Giovanna Bosshard from Institute of Pharmacology and Toxicology—Morphological and Behavioral Neuroscience (University of Zurich, CH) for kindly providing us with dissected rat hippocampi.

D. O. and L. D.-C. contributed equally to this work.

*zambelli@biomed.ee.ethz.ch

- [1] G. Binnig, C. Quate, and C. Gerber, *Phys. Rev. Lett.* **56**, 930 (1986).
- [2] W. Häberle, J. K. H. Hörber, F. Ohnesorge, D. P. E. Smith, and G. Binnig, *Ultramicroscopy* **42–44**, 1161 (1992).
- [3] C. Le Grimellec, E. Lesniewska, M. C. Giocondi, E. Finot, V. Vié, and J. P. Goudonnet, *Biophys. J.* **75**, 695 (1998).
- [4] P. Hansma, B. Drake, O. Marti, S. Gould, and C. Prater, *Science* **243**, 641 (1989).
- [5] Y. E. Korchev, M. Milovanovic, C. L. Bashford, D. C. Bennett, E. V. Sviderskaya, I. Vodyanoy, and M. J. Lab, *J. Microsc.* **188**, 17 (1997).
- [6] J. Rheinlaender and T. E. Schäffer, *J. Appl. Phys.* **105**, 094905 (2009).
- [7] J. Seifert, J. Rheinlaender, P. Novak, Y. E. Korchev, and T. E. Schäffer, *Langmuir* (2015) **31**, 6807 (2015).
- [8] D. Pastré, H. Iwamoto, J. Liu, G. Szabo, and Z. Shao, *Ultramicroscopy* **90**, 13 (2001).
- [9] P. Novak, C. Li, A. I. Shevchuk, R. Stepanyan, M. Caldwell, S. Hughes, T. G. Smart, J. Gorelik, V. P. Ostanin, M. J. Lab, G. W. J. Moss, G. I. Frolenkov, D. Klenerman, and Y. E. Korchev, *Nat. Methods* **6**, 279 (2009).
- [10] S. A. Mann, G. Hoffmann, A. Hengstenberg, W. Schuhmann, and I. D. Dietzel, *J. Neurosci. Methods* **116**, 113 (2002).
- [11] P. Happel and I. D. Dietzel, *J. Nanobiotechnology* **7**, 7 (2009).
- [12] S. Ito and F. Iwata, *Jpn. J. Appl. Phys.* **50**, 08LB15 (2011).
- [13] S. An, K. Lee, B. Kim, H. Noh, J. Kim, S. Kwon, M. Lee, M.-H. Hong, and W. Jhe, *Rev. Sci. Instrum.* **85**, 033702 (2014).
- [14] S. An, C. Stambaugh, G. Kim, M. Lee, Y. Kim, K. Lee, and W. Jhe, *Nanoscale* **4**, 6493 (2012).
- [15] A. Castellanos-Gomez, N. Agrait, and G. Rubio-Bollinger, *Nanotechnology* **20**, 215502 (2009).
- [16] K. Lieberman, A. Lewis, G. Fish, S. Shalom, T. M. Jovin, A. Schaper, and S. R. Cohen, *Appl. Phys. Lett.* **65**, 648 (1994).
- [17] S. Shalom, K. Lieberman, A. Lewis, and S. R. Cohen, *Rev. Sci. Instrum.* **63**, 4061 (1992).
- [18] M. Böcker, B. Anczykowski, J. Wegener, and T. E. Schäffer, *Nanotechnology* **18**, 145505 (2007).
- [19] B. Drake, C. Randall, D. Bridges, and P. K. Hansma, *Rev. Sci. Instrum.* **85**, 083706 (2014).
- [20] A. Meister, M. Gabi, P. Behr, P. Studer, J. Vörös, P. Niedermann, J. Bitterli, J. Polesel-Maris, M. Liley, H. Heinzelmann, and T. Zambelli, *Nano Lett.* **9**, 2501 (2009).
- [21] J. E. Sader, J. W. M. Chon, and P. Mulvaney, *Rev. Sci. Instrum.* **70**, 3967 (1999).
- [22] D. Ossola, M.-Y. Amarouch, P. Behr, J. Vörös, H. Abriel, and T. Zambelli, *Nano Lett.* **15**, 1743 (2015).
- [23] G. Meyer and N. M. Amer, *Appl. Phys. Lett.* **53**, 1045 (1988).
- [24] See Supplemental Material at <http://link.aps.org/supplemental/10.1103/PhysRevLett.115.238103>, which includes Refs. [25–28]. Detailed materials and methods. Simultaneous AFM-SICM approach on different substrates. SICM approach with different aperture sizes. Simulation of the SICM resolution with FluidFM probes. Complementary images to the figures in the Letter. High-speed SICM. Dc vs. ac SICM. Simulation of the double controller.
- [25] S. Kaech and G. Banker, *Nat. Protoc.* **1**, 2406 (2006).
- [26] G. J. Brewer, J. R. Torricelli, E. K. Evege, and P. J. Price, *J. Neurosci. Res.* **35**, 567 (1993).
- [27] H. Nitz, J. Kamp, and H. Fuchs, *Probe Microsc.* **1**, 187 (1998).
- [28] D. Thatenhorst, J. Rheinlaender, T. E. Schäffer, I. D. Dietzel, and P. Happel, *Anal. Chem.* **86**, 9838 (2014).
- [29] K. Ishizaki, T. Ushiki, M. Nakajima, and F. Iwata, in *2013 International Symposium on Micro-NanoMechatronics and Human Science (MHS)* (IEEE, Nagoya, 2013), p. 1.
- [30] E. J. W. Berenschot, N. Burouni, B. Schurink, J. W. van Honschoten, R. G. P. Sanders, R. Truckenmuller, H. V. Jansen, M. C. Elwenspoek, A. A. van Apeldoorn, and N. R. Tas, *Small* **8**, 3823 (2012).
- [31] O. Guillaume-Gentil, E. Potthoff, D. Ossola, P. Dörig, T. Zambelli, and J. A. Vorholt, *Small* **9**, 1904 (2013).
- [32] A. I. Shevchuk, G. I. Frolenkov, D. Sánchez, P. S. James, N. Freedman, M. J. Lab, R. Jones, D. Klenerman, and Y. E. Korchev, *Angew. Chem., Int. Ed. Engl.* **45**, 2212 (2006).
- [33] J. Rheinlaender and T. E. Schäffer, *Anal. Chem.* **87**, 7117 (2015).
- [34] S. Del Linz, E. Willman, M. Caldwell, D. Klenerman, A. Fernández, and G. Moss, *Anal. Chem.* **86**, 2353 (2014).
- [35] P. Novak, A. Shevchuk, P. Ruenraroengsak, M. Miragoli, A. J. Thorley, D. Klenerman, M. J. Lab, T. D. Tetley, J. Gorelik, and Y. E. Korchev, *Nano Lett.* **14**, 1202 (2014).